J Appl Electrochem (2010) 40:357–364
DOI 10.1007/s10800-009-0004-2

ORIGINAL PAPER

Structural and photoelectrochemical characterization of oxide films formed on AISI 304 stainless steel

N. E. Hakiki

Received: 7 December 2008 / Accepted: 20 August 2009 / Published online: 30 August 2009

Abstract The structural and photoelectrochemical characterization of thermally grown oxide films on stainless steel is performed by near field microscopy and photocurrent measurements. The results show that the film formed at highest temperature has a very small grain size with a small surface roughness. A decrease of the grain size with increasing temperature is obtained. The images obtained on oxide formed at low temperature show that the film compactness decreases with temperature especially at 50 °C where the film is partially formed. The results obtained by photocurrent measurements show an increase of the quantum efficiency with temperature. A band gap energy value around 2.3 eV is obtained whatever the nature of the film obtained. Plots of the quantum efficiency as a function of the energy incident light reveal the existence of a photocurrent peak located in the band gap region, at 1.9 eV, near the conduction band. The analysis of the photocurrent as a function of the applied potential reveals a Pool–Frenkel effect. The donor densities extracted from photoelectrochemical measurements are compared to those obtained in previous works by capacitance measurements. The investigation shows that the electronic structure of oxide films formed on stainless steel can be described on the basis of the band structure model developed for crystalline semiconductor materials.

Keywords Stainless steel · Atomic force microscopy · Roughness · Thickness · Photocurrent · Band gap energy · Quantum efficiency · Pool–Frenkel effect · Donor densities · Oxide · Temperature

N. E. Hakiki (✉)
Laboratoire de Physique des Couches Minces et Matériaux pour l'Electronique (LPCMME), Département de Physique, Faculté des Sciences, Université d'Oran Es-sénia, Oran 31100, Algeria
e-mail: hakiki.noureddine@yahoo.fr

1 Introduction

The study of the properties of thin passive and thick oxide films formed on stainless steel, which can be considered as the key parameters controlling the behaviour of the metal–solution interface, is still of fundamental and practical importance in corrosion science [1–12]. The investigation of these properties helps us understand the metal corrosion and the kinetics of charge transfer at the oxide film–electrolyte interface. Furthermore, a possible correlation of the corrosion resistance resulting from the formation of oxide films with their solid-state electronic characteristics can be obtained. However, a clear correlation between the film structure and its stability has never been established since the exact electronic structure of these films is not fully known. It has been shown that the electrochemical behaviour of oxides is, in several points of view, similar to that of semiconductors [13–16]. Accordingly, the concepts of semiconductor electrochemistry have been translated and used to describe the oxide properties in terms of band structure. It is a matter of fact that the application of a simplified band structure model adopted for single crystal semiconductors can appear inappropriate. Moreover, it has been shown that the semiconducting properties of these films can be investigated on the basis of a simplified energy level diagram which seems useful and accurate within proper limits [17–19]. In practice, several investigations have been performed, by "in situ" techniques such as capacitance, impedance, and photocurrent measurements [20–44]. These investigations conducted on oxide and passive films formed in different environments on alloys containing iron, chromium and nickel, such as stainless steels and nickel-based alloys reveal the semiconducting character of these films. The principles of the band theory of solids have been used quite successfully to interpret the

results obtained. Thus, solid-state properties of passive and oxide films formed in solution have been determined and, whenever possible, correlated with the stability of passive films [23]. The oxide films formed on stainless steel and alloys are generally composed by two distinctive regions of different chemical composition and semiconductivity type. These explanations are supported by the analytical results obtained by Auger Electron Spectroscopy (AES) [28, 45] and semiconducting studies [20–24]. In the first case, the quantitative approach shows that the oxide film is chemically composed of an inner layer of chromium oxide and an outer layer of iron oxide. In the second case, the results obtained show that the two oxides form a p–n heterojunction formed by an inner region of chromium oxide with *p*-type semi-conductivity [35, 46–50] and an outer region of iron oxide with *n*-type semiconductivity [40–42, 51–53]. The amount of nickel oxide found in the films does not significantly influence this heterojunction. However, the exact band structure model, which takes into account both the electronic transfer and the ionic transport of charges, might be very complicated. In the case of thermally grown oxide films, it is assumed that the inner region consists of a mixed iron-chromium spinel oxide $(Fe_{2-x}{}^{3+}Cr_x{}^{3+}Fe^{2+})O_4{}^{2-}$ with $0 \leq x \leq 2$ [54]. This value of x which is influenced by the formation temperature of the film increases with temperature decay. The oxide layers formed at room temperature are highly disordered and resemble more to amorphous materials than crystalline ones. Their properties with respect to conductivity, mass transport and light absorption will vary to a large extent depending on the conditions of their formation. Understanding the influence of the electronic structure of the passive and oxide films on the corrosion resistance of stainless steels implies the ability to describe, not only the space charges created at both metal/film and film/electrolyte interfaces and also the n–p heterojunction situated in the internal part of the film. The composition of these layers with regard to disorder and doping level is usually not uniform. Therefore, the electronic properties vary with thickness and distance from the metal. This affects seriously the charge distribution with and without applied bias, the more so under illumination. Further complications are related to the fact that in many practical applications, the oxide films grown on alloys are not homogeneous both at large as well as at microscopic scale so that the information obtained is often qualitative.

Photoelectrochemical technique is used to investigate optical and electronic properties of semiconductor electrodes as bulk materials [55–60] and to characterize passive and oxide layers on metals [52, 61–64]. Optical excitation with energy light larger than the band gap leads to the formation of electrons and holes that are separated by the high field, with one species migrating to the surface where it may react with solution species to give a photocurrent. "In situ" photoelectrochemical methods are extended for thin oxide films with semiconducting properties. The photoelectrochemical behaviour of oxide films is largely influenced by their electronic properties as the excitation of current by light provides much information on electronic structure in the oxide layer. Consequently, extended photo electrochemical method can be used as an important "in situ" technique to characterize oxide films. For this reason, photoelectrochemistry is becoming one of the most used and adapted methods for studying passive and oxide films formed on stainless steels and nickel-based alloys. In fact, the analysis of the photocurrent created through photon–mater interaction enables the access to different parameters characterizing their band structure and their semiconducting properties.

The purpose of this article is to obtain a more detailed information about the structural and photoelectrochemical characterization of the films formed on AISI 304 stainless steel with a particular emphasis on the influence of formation temperature. The photoelectrochemical properties via photocurrent measurements are reported in order to study the influence of formation temperature on the electronic structure of the oxide films formed on the alloy. The results of these measurements lead to a better understanding of the solid-state properties of the oxide films formed on stainless steels.

2 Experiments

Austenitic type AISI 304 stainless steel of composition (wt%) (Cr: 17.4; Ni: 8.3; C: 0.053; N: 004; Si: 0.48; Mn: 1.42; Mo: 0.39; Cu: 0.14) is used for the test species. The samples, of surface area 0.8 cm^2 are annealed for 30 min. at 1050 °C. Then, they are abraded with wet SiC paper of different grit size, finally polished with alumina 2 μm, rinsed in distilled water, ultrasonically cleaned and dried with air. Oxidation of the samples was made in air, at controlled and selected temperatures ranging between 50 to 450 °C, inside a furnace, for 2 h at atmospheric pressure. AFM images were recorded using the near field microscopy JEOL JSPM 4200 system.

Atomic force microscopy (AFM) is a method of measuring the surface topography on a scale from angstroms to 100 μ. The technique involves imaging a sample through the use of a probe, or tip, with a radius of 20 nm. The tip is held several nanometers above the surface using a feedback mechanism that measures surface–tip interactions on the nano Newtons scale. Variations in tip height are recorded while the tip is scanned repeatedly across the sample, producing a topographic image of the surface. The key to the sensitivity of AFM is in monitoring the movement of

the tip. As in STM method, rastering the tip across the surface produces a topographic map of the surface with atomic resolution. Scanning-tunneling microscopy (STM) can image surfaces of conducting materials with atomic-scale resolution. It uses an atomically sharp metal tip that is brought very close to the surface.

For electrochemical measurements, a classical cell with three electrodes is used with a platinum counter-electrode (area = 1 cm^2) and a saturated calomel electrode (SCE) as reference. All experiments were carried out at room temperature (22 °C) under continuous high purity nitrogen bubbling in a buffer solution of composition H_3BO_3 (0.05 M) + $Na_2B_4O_7{\cdot}10H_2O$ (0.075 M) leading to pH = 9.2. The specimens previously oxidized were immersed in the solution and left at rest potential for 2 h before measurements were taken. Photoelectrochemical measurements were performed using a 150 W xenon lamp and a 1,200/mm grating monochromator (Jobin-Yvon H25). The photocurrent is generated by focusing the light with a fused silica lens through a quartz window of the electrochemical cell onto the working electrode. The lock-in technique using a double phase synchronous detector (Brookdeal 5208 lock-in amplifier) is used. This technique allows separation of the photocurrent from the sample current by chopping the light at a constant frequency (19 Hz) and feeding the signal as well as the current output of the potentiostat (PAR 273) to the lock-in amplifier. The photocurrent spectra are obtained by scanning the light wavelength in steps of 50 nm from 750 to 250 nm. The dependence of the photocurrent on the applied potential U is obtained at a fixed wavelength (350 nm) by scanning successively the applied potential in steps of 50 mV in the potential range 1 to −1.5 V. The photocurrent action spectra are corrected for the lamp efficiency without t aking into account the reflections at the film–solution interface.

3 Results and discussion

3.1 Structural characterization

Figure 1 presents AFM images of oxide films formed on AISI 304 stainless steel at different temperatures (a: 350 °C, b: 150 °C and c: 50 °C). It appears clearly that the film formed at highest temperature (350 °C) has a very small grain size, a small surface roughness and that the grain size decrease with increasing temperature. The images obtained on oxide formed at lower temperatures (150 °C and 50 °C) show that the compactness of the film decreases with formation temperature especially at lowest temperature (50 °C), where the film is partially formed. These considerations influence the optical and the semiconducting properties of the oxide film. Moreover, the contrast seen in these images appears to indicate an increase in grain size in the deeper parts of the films. However, pair of high magnification AFM images from the same region type shows that what appear to be large individual grains in the deeper part of the films is more often agglomerations of smaller side particles. There are also present, individual particles down to a size about 10 nm or smaller, which were simply invisible at lower resolution. The outer part of the oxide shows no such subdivisions at higher magnification. The initial conclusion is thus reversed, with the grain size apparently decreasing with depth. A few comments on these results are necessary. First, the AFM at this resolution gives direct crystallographic information about the object. The conclusion that what are seen in the higher magnification AFM images are individual grains might therefore be questioned. Some overestimations of grain-sizes by the near field microscopes have previously been observed and various explanations given [65]. This is a fact which is very easily missed in AFM where an observer recording an image would be tempted to presume that it was representative of the entire surface. It is difficult to operate the AFM at lower magnification and still have the definition to see the grains on this type of material. Thus the images shown here are 'typical' but other regions exist in which the average grain size may be a factor of 2 or 3 bigger or smaller. To be more quantitative, we determine the surface roughness parameter named RMS using appropriate imaging software as a function of the formation temperature. The parameter RMS is calculated using the following expression:

$$\mathrm{RMS} = \sqrt{\frac{1}{512}\sum_{i=1}^{512}\left[h(x_i, y_i, t) - E_p(t)\right]^2} \quad (1)$$

where $E_p(t) = \frac{1}{512}\sum_{i=1}^{512} h(x_i, y_i, t)$. is the mean height of the height distribution.

Figure 2 shows the dependence of surface roughness on increasing formation temperature. The RMS value increases slowly when temperature increases up to 200 °C, then a drastic change in the surface state occurs near 100 °C. For a temperature higher than this value, the RMS value reaches a saturation value near 90 nm. One can observe that the calculated roughness is the sum of two contributions, the roughness due to the oxidation process and the roughness due to the polishing process. At high temperature, the RMS factor is dominated by the grain like morphology of the oxide layer, whereas at lower temperature, the RMS value reflects mostly the stripes due to the polishing process. However, it appears also on this figure that the oxide grains shape is influenced by the density and thickness of the stripes.

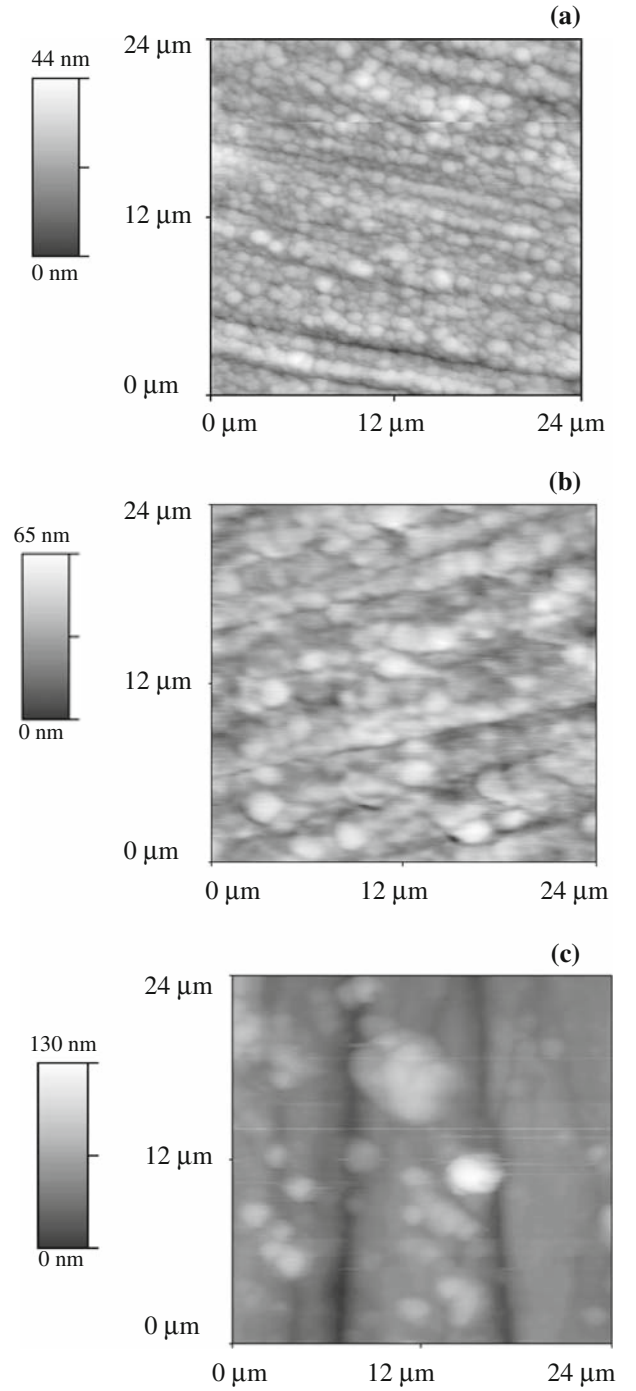

Fig. 1 AFM microscopy images of oxide films formed at different temperatures: **a** 350 °C, **b** 150 °C, **c** 50 °C

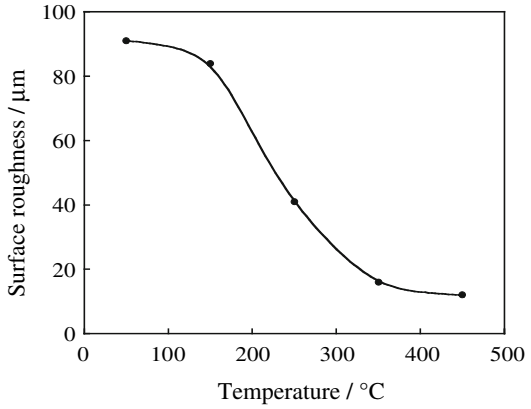

Fig. 2 Plot of RMS surface roughness versus formation temperature

3.2 Photoelectrochemical characterization

Photoelectrochemistry at semiconductor electrodes is widely reviewed in literature. In the recent years, this technique has been shown to be a valuable tool, despite the fact that it is not always a simple technique for characterizing oxide and passive films on metals and alloys in terms of electro-optical properties. Information can be obtained on the chemical nature of these layers, as well as on the energetic diagram of the film/electrolyte interface [20, 21, 25, 26, 29, 66–77]. The interpretation of the results in these works requires often the extension and modifications of models usually employed in the case of crystalline semiconductors. When a radiation of sufficient quantum energy is absorbed by a semiconductor or an insulator, a photocurrent is generated. The effect of light is primarily to increase the density of the free charge carriers. The photocurrent depends upon how long these carriers can remain free before recombining, i.e. upon their lifetime. Thus, the presence of electrical barriers promoted by space charges can facilitate or hinder recombination [58].

Assuming that the recombination of photo-generated charge carriers can be neglected, the photocurrent response of a semiconductor can be described quantitatively by the Gärtner and Butler equation [66, 67]

$$I_{ph} = e\Phi_0\left[1 - \frac{\exp(-\alpha W_{SC})}{1 + \alpha L_P}\right] \quad (2)$$

where I_{ph} is the photocurrent, e the charge of the electron, Φ_0 the incident photon flux, α the absorption coefficient, L_P the hole diffusion and W_{SC} the space charge layer thickness. This last parameter is related to the applied potential, U, and the flat band potential, U_{FB}, by

$$W_{SC} = \left[\frac{2\varepsilon\varepsilon_0}{eN_D}\right]^{0.5}\left(U - U_{FB}\right)^{0.5} \quad (3)$$

where ε and ε_0 are the dielectric constant and the vacuum permittivity, respectively. N_D is the donor concentration for a *n*-type semiconductor.

For $\alpha L_P \ll 1$ and $\alpha W_{SC} \ll 1$, i.e. a small hole diffusion length and a small space charge layer thickness, which is the case for the majority of oxide films formed on metals and alloys, Eq. 2 can be simplified to

$$I_{ph} = e\Phi_0\alpha[L_P + W_{SC}] \quad (4)$$

For many semiconductors, it has been found that the relation between photon energy and the absorption coefficient α, is given by

$$\alpha hv = A\left(hv - E_g\right)^n \quad (5)$$

where E_g is the band gap energy, A is a constant and $n = 0.5$ for direct transitions and $n = 2$ when indirect transitions are considered. In terms of quantum efficiency, η is defined as the ratio of the photocurrent by the incident photon flux. The dependence of the photo response on energy and space charge layer thickness becomes

$$\eta hv = A[L_P + W_{SC}]\left(hv - E_g\right)^n \quad (6)$$

This relation can be used to determine the band gap energy.

Experimentally, photoelectrochemical behaviour of passive and oxide films can be investigated by determining the photocurrent, generated under illumination, as a function of incident light energy and applied potential. The measurements conducted on these films at different frequencies of the modulated light reveal its frequency dependence. Thus, in all cases, the measurements are performed at 19 Hz, which approximately corresponds to the stationary photocurrent.

The analysis of the photocurrent spectra shows that $n = 2$ is the most appropriate value to represent the photoelectrochemical behaviour observed. This value which corresponds to indirect transitions in crystalline band structure model has been obtained in different previous works on passive films [68, 69]. The same value ($n = 2$) has been also predominantly obtained with amorphous materials where the transitions are called non-direct.

Figure 3 shows the photocurrent spectra obtained with the oxides formed at different temperatures. The spectral response of all films was essentially similar in shape and wavelength region, disregarding some minor differences. As can be observed, the value of the quantum efficiency increases with the temperature of oxidation treatment.

In Fig. 3, the slope of $(\eta hv)^{0.5}$ versus hv plots can be determined in the energy range where a linear behaviour is manifested. These slopes (called β) are recorded as a function of temperature formation in Fig. 4 where the oxide thickness obtained by quantitative auger analysis [20, 26] are also reported. It clearly appears that these variations were essentially similar in shape and temperature region. The increase with temperature revealed by both β and oxide thickness is in accordance with an enlargement of the space charge layer of the films which can be related to their thickness. This can be explained if it is assumed that a decrease of donor density corresponds to a diminution of film defects and consequently electron-hole recombination processes. In this case, the decrease of the quantum

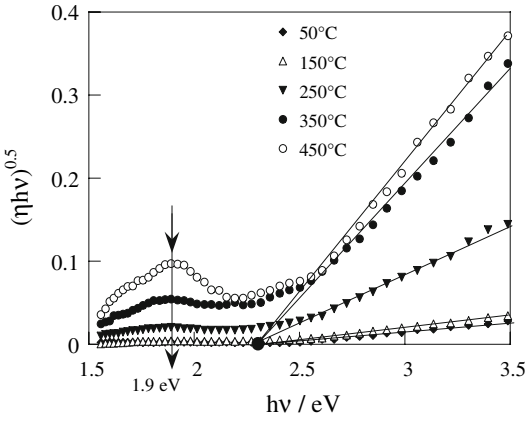

Fig. 3 Plots of $(\eta hv)^{0.5}$ versus hv for the different oxide films formed at different temperature

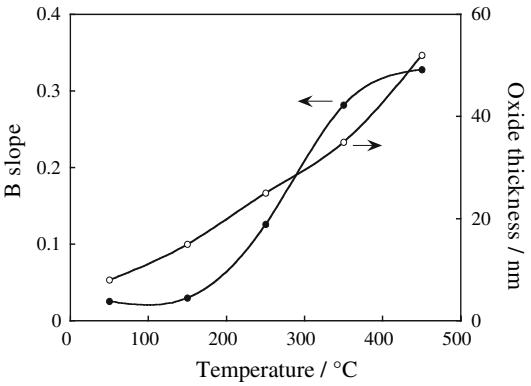

Fig. 4 Plot of β slope and oxide thickness versus formation temperature

efficiency in films formed at lower temperatures may result from the recombination processes which become more important when the number of defects within the film increases. Moreover, it is obvious from Eq. 6 that a direct relationship between the thickness of the space charge layer, W_{SC}, and the quantum efficiency, η exists, but the physical description given above is not straightforward from the equation. Moreover, according to the Gärtner model, an increase in the photocurrent can result from photon-generated charge carriers that reach the space charge region by diffusion from the underlying diffusion layer region, whose width increases with film thickness [25].

By extrapolation of $(\eta hv)^{0.5}$ to $hv = 0$ in Fig. 3, a threshold energy value of 2.3 eV is obtained for all the oxide films. This value is in excellent agreement with reported band gap values of passive films formed on stainless steels. Furthermore, several measurements demonstrate an excellent reproducibility of the photocurrent spectra obtained for the different oxide films. Figure 3 also reveals the existence of a peak in photocurrent situated at

1.9 eV in the sub band gap region. This peak can be associated with transitions from the valence band to the second donor level localised in the band gap. Thus, taking into account the fact that the energy band gap value is 2.3 eV, it can be easily established that this level is situated at 0.4 eV below the conduction band. This means that excitation is possible from the valence band to localized states in the band gap of the oxide film, which can be related to the crystallographic structure. It also appears that the quantum efficiency for sub band gap photon energies decreases with the temperature of oxidation treatment. Since the oxide films are considered as highly disordered, the existence of traps in the band gap has been suggested by many workers [20–24]. It should be noted that the results presented above illustrate the high sensitivity of the photo electrochemical technique and the equipment used.

The Pool–Frenkel effect describes the influence of the electric field, F, on the escape probability, P_i, of the electron from a trap where it is bound by coulumbic interactions. When an electric field is superimposed on the trap, the escape barrier is lowered by an amount $\beta F^{0.5}$ and P_i is given by the Pool–Frenkel equation [78]

$$P_i = \exp\frac{-E_i + \beta F^{0.5}}{kT} \tag{7}$$

where E_i is the ionization energy, i.e. the energy difference between the lower edge of the conduction band and the trap, k being the Boltzmann constant, T the temperature and $\beta = \left(\frac{e^3}{\varepsilon\varepsilon_0\pi}\right)^{0.5}$.

Since the photocurrent, I_{ph}, is proportional to the escape probability, it can be written as

$$I_{ph} = A' \exp\left(\frac{-E_i + \beta F^{0.5}}{kT}\right) \tag{8}$$

where A' is a constant

Assuming that the electric field, F, is related to the applied potential, U, and the flatband potential, U_{FB}, by

$$F = \frac{U - U_{FB}}{W_{SC}} \tag{9}$$

where the space charge layer thickness is given by Eq. 3, the photocurrent is given by

$$I_{ph} = A' \exp\left(\frac{-E_i + \beta W_0^{0.5}(U - U_{FB})^{0.25}}{kT}\right) \tag{10}$$

In logarithmic representation, the quantum efficiency is given by

$$Ln\eta = Ln\frac{A'}{e\Phi_0} - \frac{E_i}{kT} + \frac{1}{kT}\left(\frac{e^3}{\varepsilon\varepsilon_0\pi}\right)^{0.5}\left(\frac{eN_D}{2\varepsilon\varepsilon_0}\right)^{0.25}(U - U_{FB})^{0.25} \tag{11}$$

According to Eq. 11, $Ln(\eta)$ versus $(U - U_{FB})^{0.25}$ plots would reveal a linear variation, with a slope depending on the donor density, N_D, and the dielectric constant, ε.

The potential dependence of the photocurrent can be especially different if localized states are involved. An exponential type of potential dependence according to Pool–Frenkel effect can be expected. The results show that the excitation is possible from the valence band to localized states in the band gap of the oxide present in the oxide film. The photocurrent obtained in the sub band gap region is most probably determined by hopping or tunnels processes. Electron transition from the deep donor level to the conduction band may also occur. In the case of a classical semiconductor, traps can drastically change the charge distribution and reduce the quantum yield. It appears that in these points, the behaviour of the oxide films is quite similar. The study of localized states in the band gap implicitly yields valuable information on the nature of the donor species from a structural and chemical point of view. Previous works describe the sub band gap response near the conduction band as a characteristic behaviour of amorphous materials (the Urbach tail). The present result shows that this phenomenon may result from localized traps in the band gap. Such behaviour is necessarily a consequence of the presence of short range crystalline order. This analysis disagrees with the idea that the structure of the film may be closer to that of an amorphous rather than crystalline solid. It also appears that the oxide films show a greater degree of covalence in bonding than standard crystalline oxides. Thus, if we consider that the essential crystallographic factor characteristic of bulk oxides exist in the oxide films, the familiar concepts of semiconductor electrochemistry can be applied. At fixed wavelength and variable potential, the photoresponse becomes governed by the variation in the band bending created by electrochemical polarization and reflects the behaviour of the space charge layer under illumination. Experimentally, this kind of information can be obtained only if the energy of incident light is greater than the band gap energy. At $\lambda = 370$ nm, where the photocurrent spectra present maximum intensity, the photocurrent was measured as a function of the applied potential. These measurements reflect the characteristic dependence of the depletion layer thickness on the potential and are analogous to Mott-Schottky behaviour. Using the values of the flat band potentials ($U_{FB} = -0.5$ V/sce) extracted from capacitance results obtained on the same oxide films [20, 26], we have represented, in Fig. 5, $Ln(\eta)$ versus $(U - U_{fb})^{0.25}$ for the different oxide films. The straight lines obtained in concordance with Eq. 11 indicate that the Pool–Frenkel effect is a reasonable model to describe the photocurrent-potential dependence in these oxide films. This figure shows that all the oxide films

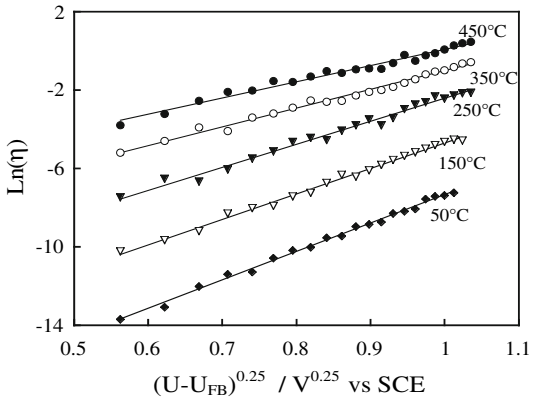

Fig. 5 Plot of $Ln(\eta)$ versus $(U - U_{FB})^{0.25}$ for the different oxide films formed at different temperature

exhibit the same photoelectrochemical behaviour. This is due to the fact that this region is controlled essentially by the iron oxide whatever the film considered. Quantitatively, the photoresponse is closely related to the formation temperature. A decrease of the quantum efficiency with the temperature of oxidation treatment is also obtained, a result in agreement with those obtained in Fig. 3.

From the slopes of $Ln\ (\eta)$ versus $(U - U_{fb})^{0.25}$ plots and Eq. 11, the donor densities can be evaluated quantitatively for a given ε or vice versa. Using $\varepsilon = 12$ for the dielectric constant of iron oxide [41–43, 53–55], we have determined the donor densities for the oxide films which are represented for different temperatures and compared to those obtained in previous work [20, 26] by capacitance measurements (Fig. 6).

In both cases, the donor densities present qualitatively the same variation versus oxidation treatment temperature, i.e. an increasing with temperature. This increase can be due to defect structure which becomes more important and reduction of space charge layer thickness when the temperature of oxidation treatment temperature decreases. Quantitatively the values of N_D obtained by photoelectrochemical

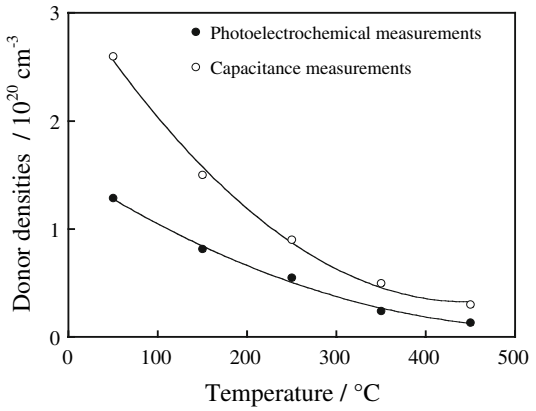

Fig. 6 Plot of donor densities versus the formation temperature

measurements are lower than those determined by capacitance measurements. Nevertheless, the ratio of the donor densities obtained by both methods is approximately constant. Several effects can be suggested to explain the difference between the values of N_D determined by the two types of techniques. First, the reflection of the light at the film–metal interface can also introduce a change in the value of N_D. Indeed, the width of the space charge layer should be considered twice and according to Eq. 10, it increases the value of N_D. Second, the hopping mechanism can also promote a deviation of N_D from values obtained from capacitance measurements. Finally, the most probable effect is without doubt related to the fact that the capacitance and the photocurrent are frequency dependent. The values of the donor densities are extracted from the capacitance and the photocurrent measured at high and low frequency, respectively. Therefore, the ionic migration processes and the surface states can strongly contribute to photoelectrochemical measurements.

4 Conclusion

In this study, we have combined structural and photoelectrochemical techniques in an attempt to characterize the properties of protective oxide layers. The results of these measurements have led to a better understanding of the solid-state properties of the oxide films formed on stainless steel, and at the same time have helped to clarify the effect of formation temperature. The microscopic characterization shows that the film formed at highest temperature (350 °C) has a very small grain size with a small surface roughness and that the grain size decrease with increasing temperature. The compactness of the film also decreases with formation temperature especially at lowest temperature (50 °C) where the film is partially formed. The RMS value varies slowly at high and low temperatures but presents drastic variation in the intermediary interval (150 °C – 350 °C). The photoelectrochemical study presented shows that the electronic structure of the thermally grown oxide films on stainless steel can be described on the basis of the band structure model developed for crystalline semiconductor materials. The existence of band gaps, space charge regions and donor levels can characterize oxide films. The quantum efficiency is closely related to the formation temperature of the films. However, the band gap value is constant whatever the nature and the thickness of the film. Plots of the quantum efficiency η as a function of energy incident light reveal the existence of a photocurrent peak at 1.9 eV located in the band gap region near the conduction band. Based on the photoelectrochemical results obtained, it is possible to present a more accurate picture of the electronic structure of the oxide

films formed on stainless steel and to discuss the manner in which the formation conditions affect this structure.

References

1. Hakiki NE (2008) J Appl Electrochem 38:679–687
2. Hakiki NE, Maachi B (2007) Phys Chem News 38:65–69
3. Wijesinghe TLSL, Blackwood DJ (2007) J Electrochem Soc 154:C16
4. Ha HY, Park C, Kwon H (2007) Corros Sci 49:1266
5. Jang HJ, Kwon HS (2006) J Electroanal Chem 590:120
6. Kim DY, Ahn S, Kwon H (2006) Thin Solid Films 513:212
7. Jang H, Park C, Kwon H (2005) Electrochim Acta 50:3503
8. Ahn SJ, Kwon HS (2004) Electrochim Acta 49:3347
9. Cho EA, Kwon HS, Macdonald DD (2002) Electrochim Acta 47:1661
10. Ferreira MGS, Da Cunha Belo M, Hakiki NE, Goodlet G, Montemor MF, Simões AMP (2002) J Braz Chem Soc 13:433
11. Kim JS, Cho EA, Kwon HS (2001) Corros Sci 43:1403
12. Kim JS, Cho EA, Kwon HS (2001) Electrochim Acta 47:415
13. Stimming U (1986) Electrochim Acta 31:415
14. Schmuki P, Bohni H (1992) J Eleclrochem Soc 139:1908
15. Schmuki P, Bückler M, Virtanen S, Böhni H, Müller R, Gauckler LJ (1995) J Electrochem Soc 142:3336
16. Searson PC, Latanision RM, Stimming U (1988) J Electrochem Soc 135:1358
17. Chen CT, Cahan BD (1982) J Electrochem Soc 129:17
18. Sato N, Kudo K, Noda T (1971) Electrochim Acta 16:1909
19. Gerischer H (1989) Corros Sci 29:191
20. Hakiki NE, Montemor MF, Ferreira MGS, Da Cunha Belo M (2000) Corros Sci 42:687
21. Montemor MF, Ferreira MGS, Hakiki NE, Da Cunha Belo M (2000) Corros Sci 42:1635
22. Da Cunha Belo M, Walls M, Hakiki NE, Corset J, Picquenard E, Sagon G, Nöel D (1998) Corros Sci 40:447
23. Da Cunha Belo M, Rondot B, Compere C, Montemor MF, Simöes AMP, Ferreira MGS (1998) Corros Sci 40:481
24. Hakiki NE, Boudin S, Rondot B, Da Cunha Belo M (1995) Corros Sci 37:1809
25. Di Paola A, Di Quarto F, Sunseri C (1986) Corros Sci 26:935
26. Ferreira MGS, Hakiki NE, Goodlet G, Faty S, Simöes AMP, Da Cunha Belo M (2001) Electrochim Acta 46:3767
27. Da Cunha Belo M, Hakiki NE, Ferreira MGS (1999) Electrochim Acta 44:2473
28. Simöes AMP, Ferreira MGS, Lorang G, Da Cunha Belo M (1991) Electrochim Acta 36:315
29. Di Paola A (1989) Electrochim Acta 34:203
30. Hakiki NE, Da Cunha Belo M, Simöes AMP, Ferreira MGS (1999) J Electrochem Soc 146:807
31. Hakiki NE, Da Cunha Belo M, Simöes AMP, Ferreira MGS (1998) J Electrochem Soc 145:3821
32. Schmuki P, Virtanen S, Isaacs HS, Ryan MP, Davenport AJ, Böhni H, Stenberg T (1998) J Electrochem Soc 145:791
33. Hakiki NE, Da Cunha Belo M (1996) J Electrochem Soc 143:3088
34. Simöes AMP, Ferreira MGS, Rondot B, Da Cunha Belo M (1990) J Electrochem Soc 137:82
35. Sunseri C, Piazza S, Di Quarto F (1990) J Electrochem Soc 137:2411
36. Schmuki P, Böhni H (1989) J Electrochem Soc 139:7
37. Sunseri C, Piazza S, Di Paola A, Di Quarto F (1987) J Electrochem Soc 134:2410
38. Hakiki NE, Da Cunha Belo M (1995) CR Acad Sci Paris 320(II):613
39. Hakiki NE, Da Cunha Belo M (1993) CR Acad Sci Paris 317(II):457
40. Delnick FM, Hackermann N (1979) J Electrochem Soc 126:732
41. Azumi K, Ohtsuka T, Sato N (1987) J Electrochem Soc 134:1352
42. Stimming U, Schultze JW (1976) Ber Bunsenges Phys Chem 8:129
43. Stimming U (1987) Langmuir 3:423
44. Dean MH, Stimming U (1987) J Electroanal Chem 228:135
45. Lorang G, Da Cunha Belo M, Simões AMP, Ferreira MGS (1994) J Electrochem Soc 141:3347
46. Lillerud KP, Kofstad P (1980) J Electrochem Soc 127:2397
47. Blazey KW (1972) Solid State Commun 11:317
48. Young EWA, Gerretsen JH, de Wit JHW (1987) J Electrochem Soc 134:2257
49. Dare-Edwards MP, Goodenough JB, Hamnett A, Nicholson ND (1981) J Chem Soc Faraday Trans 2:643
50. Wilhelm SM, Hackerman N (1981) J Electrochem Soc 128:1668
51. Stimming U (1983) In: Froment M (ed) Passivity of metals and semi-conductors. Elsevier, Amsterdam, p 477
52. Schultze JW, Stimming U (1982) Ber Bunsenges Phys Chem 86:276
53. Wilhelm SM, Yun KS, Ballanger LW, Hackermann N (1979) J Electrochem Soc 126:419
54. Gillot B, Rousset A (1986) J Electroanal Chem 65:322
55. Wilson RH (1977) J Appl Phys 48:4292
56. Reichmann J (1980) Appl Phys Lett 36:574
57. Reiss H (1978) J Electrochem Soc 125:937
58. Pleskov YuV, Gurevich YuYa (1986) Semiconductor photoelectrochemistry. Consultants Bureau, New York
59. Morrison SR (1980) Electrochemistry of Semiconductors and Oxidized metal Electrodes. Plenum Press, New York
60. Morrison SR (1977) The chemical physics of surfaces. Plenum Press, New York
61. Myamlin VA, Pleskov YuV (1967) Electrochemistry of semiconductors. Plenum Press, New York
62. McAlear JF, Peter LM (1980) Faraday Discuss Chem Soc 70:67
63. Di Quarto F, Di Paola A, Sunseri C (1981) Electrochem Acta 26:1177
64. Peter LM (1987) Ber Bunsenges Phys Chem 91:419
65. Rauf IA, Walls MG (1991) Ultramicrosc 127:737
66. Gärtner WW (1959) Phys Rev 116:84
67. Butler MA (1977) J Appl Phys 48:1914
68. Pankove JI (1975) Optical processes in semiconductors. Dover, NY
69. Bube RH (1967) Photoconductivity of solids. Wiley, NY
70. Hakiki NE, Simöes AMP, Ferreira MGS, Da Cunha Belo M (2000) Port Electrochim Acta 18:113
71. Montemor MF, Ferreira MGS, Hakiki NE, Da Cunha Belo M (1998) Mater Sci Forum 289:1139
72. Wilhelm SM, Hackermann N (1979) J Electrochem Soc 128:1668
73. Wilhelm SM, Tanizawa Y, Liu CY, Hackermann N (1982) Corros Sci 22:791
74. Di Quarto F, Russo G, Sunseri C, Di Paola A (1982) J Chem Soc Faraday Trans I 78:3433
75. Di Quarto F, Di Paola A, Piazza S, Sunseri C (1985) Solar Energy Mater 11:419
76. Di Quarto F, Piazza S, Sunseri C (1985) Electrochem Acta 30:3
77. Abrantes LM, Peter LM (1983) J Electroanal Chem 150:593
78. Dean MH, Stimming U (1989) Corros Sci 29:199